Engineering Notes

ENGINEERING NOTES are short manuscripts describing new developments or important results of a preliminary nature. These Notes cannot exceed 6 manuscript pages and 3 figures; a page of text may be substituted for a figure and vice versa. After informal review by the editors, they may be published within a few months of the date of receipt. Style requirements are the same as for regular contributions (see inside back cover).

A80-082

0001
0003

Radiative Melting of Materials with Melt Removal

Anant Prasad*
Regional Institute of Technology, Jamshedpur, India

Nomenclature

c	= heat capacity per unit volume of the material, kcal/m^{3}K
H	= heat flow vector, kcal/m^2
H^*	= dimensionless heat flow vector = $kcH/\epsilon\sigma T_m^2$
$\dot{H}^*$	= time rate of dimensionless heat flow vector
k	= thermal conductivity of the material, kcal/m h K
L	= latent heat of the material, kcal/kg
m	= dimensionless thickness of the melt removal = $\epsilon\sigma T_m^3 q_3/k$
$\dot{m}$	= time rate of dimensionless thickness of the melt removal
$q_1(t)$	= unknown surface temperature, K
$q_2(t)$	= unknown penetration depth, m
$q_3(t)$	= unknown thickness of melt removal, m
S_t	= inverse of Stephan number = $\rho L/cT_m$
t	= time, h
T	= temperature, K
x	= direction in which heat is applied, m
α	= thermal diffusivity of the material, m^2/h
ϵ	= emissivity of the material
σ	= Stephan-Boltmann constant, kcal/M^2 h K^4
η	= dimensionless penetration depth, $\epsilon\sigma T_m^3 q_2/k$
$\dot{\eta}$	= time rate of dimensionless penetration depth
ξ	= dimensionless direction in which heat is applied = $\epsilon\sigma T_m^3 x/k$
ρ	= density of the material, kg/m^3
θ	= dimensionless temperature = T/T_m
θ_1	= dimensionless surface temperature = q_1/T_m
τ	= dimensionless time = $\epsilon^2\sigma^2 T_m^6 t/ck$

Subscripts

a	= conditions of the surroundings
i	= initial condition
m	= condition at initiation of melting
s	= steady state

Introduction

MELTING of solids due to radiative heating with the removal of melt after its immediate formation on the surface of the solid is of importance in the design of thermal protective systems for missiles and space vehicles and in the control of the movement of consumable electrodes. The heating occurs when a large temperature difference exists between the solid and the surroundings and is preceded by melting. Although the premelt heating remains for a short time owing to the rapid buildup of surface temperature to reach the melting temperature of the solid, its effect cannot be ignored. The mathematical model for this problem is nonlinear. In the premelt heating regime, the nonlinearity is caused by the radiative heating, whereas in the melting with the melt-removal regime, it is due to radiative heating and a moving boundary. Its solution is difficult to obtain unless a finite difference solution procedure is applied. Even so, the numerical technique requires large computer time and yields numerical results that are restricted to those values of parameters for which they are calculated. Consequently, approximate analytical analyses become important. Such an analysis, called Biot's variational method, has been employed by several workers to solve the melting problems with[1-3] the removal of melt. For such a problem,[3] this method has given closed-form solutions.

The present problem is concerned with heating and melting of solids when subjected to radiative heating. The melt is removed as soon as it is formed on the surface of the solid. Using Biot's variational method, solutions are obtained in closed form for both the premelt and melt-removal heating regimes. Numerical solutions are also presented.

Theoretical Analysis

A solid body initially at a constant temperature T_i, which is less than the melting temperature T_m of the solid, is considered in the form of a semi-infinite solid of uniform cross-sectional area. The surface ($x=0$) is subjected to one-dimensional radiative heating which causes a buildup of the surface temperature and penetration of heat within the solid. If $q_1(t)$ and $q_2(t)$ denote, respectively, the surface temperature and the thermal penetration depth at time t measured from the initiation of heating, both increase with increasing time and eventually $q_1(t)=T_m$. At this temperature, the penetration depth becomes $q_{2m}(t)$. The heat transfer equation describing such a premelt heating regime ($0<t\leq t_m$) in terms of nondimensional variables takes the form

$$\partial^2\theta/\partial\xi^2=\partial\theta/\partial\tau \qquad (\xi>0,\ 0<\tau\leq\tau_m) \tag{1}$$

In this regime, the thermophysical properties of the solid are assumed to be uniform. The associated nondimensional initial and boundary conditions are

$$\theta=\theta_i \qquad (\eta=0,\quad \tau=0) \tag{2}$$

$$\partial\theta/\partial\xi=\theta_1^4-\theta_a^4 \qquad (\xi=0,\quad \theta_a>\theta_1,\quad 0<\tau\leq\tau_m) \tag{3}$$

$$\partial\theta/\partial\xi=0 \qquad (\theta=\theta_i,\quad \xi=\eta,\quad 0<\tau\leq\tau_m) \tag{4}$$

With the continued heating of the solid beyond the time ($t>t_m$) required for the surface $x=0$ to reach the melting temperature of the solid, melting occurs and the melt is removed immediately upon its formation. With $q_3(t)$ representing thickness of the melt removed at any time $t(t>t_m)$ and $q_2(t)$, the thermal penetration depth measured from the newly formed surface, the heat transfer equation in nondimensional form for the solid with constant thermophysical properties is written as

$$\partial^2\theta/\partial\xi^2=\partial\theta/\partial\tau \qquad (\xi>m,\quad \tau>\tau_m) \tag{5}$$

whereas the initial and boundary conditions are

$$\theta=1 \qquad (m=0,\quad \eta=\eta_m,\quad \tau=\tau_m) \tag{6}$$

Received Sept. 19, 1979; revision received Feb. 21, 1980.

Index categories: Heat Conduction; Ablation, Pyrolysis, Thermal Decomposition and Degradation (including Refractories).

*Assistant Professor, Department of Mechanical Engineering.

$$\theta=\theta_i \quad (\xi=m, \quad \tau=\tau_m) \tag{7}$$

$$\theta=1 \quad (\xi=m, \quad \tau>\tau_m) \tag{8}$$

$$\partial\theta/\partial\xi=0 \quad (\xi=m+\eta, \quad \tau>\tau_m) \tag{9}$$

and in the melting process,

$$(\theta_a^4-1)=[(1-\theta_i)+S_t]\dot{m}+\mathrm{d}H^*/\mathrm{d}\tau \quad (\xi=m,\tau>\tau_m) \tag{10}$$

It is noted that Eq. (10) is obtained from the fact that the heat supplied by radiative heating is equal to the heat required to melt the solid to a depth m and to raise the temperature of this layer from its initial temperature to the melting temperature, plus the heat penetration to the depth η measured from the newly formed surface. Equation (3) of the premelt heating regime and Eq. (10) of the melting process are derived on the assumption that the solid is opaque to thermal radiation.

Solution

To use Biot's variational method in both regimes, a temperature distribution in the solid is approximated by the expression

$$\theta-\theta_i=(\theta_1-\theta_i)[1-(\xi-m)/\eta]^3 \tag{11}$$

Such a cubic profile has been shown to give reliable results in earlier studies.[1-3] The surface temperature, θ_1, the thermal penetration depth η, and the depth of melt removal m act as unknown generalized coordinates in the variational method and are determined as functions of time. Equation (11) yields the temperature distribution for the melting with the melt-removal regime, where the surface temperature represents the temperature of the newly formed surface after the removal of the melt to the depth m and remains at the melting temperature of the solid. The penetration depth denotes the distance from the new surface. In the premelt heating regime, although the surface temperature rises with time, it does not exceed the melting temperature of the solid nor there is any formation of melt ($m=0$). When values for θ_1 and η are substituted in Eq. (11), it provides the temperature distribution for this regime with the penetration depth measured from $\xi=0$.

The conservation of energy in nondimensional form is

$$\mathrm{div}\, H^*=-(\theta-\theta_i) \tag{12}$$

Equation (11) together with Eq. (12) gives the heat flowfield

$$H^*=\tfrac{1}{4}\eta(\theta_1-\theta_i)[1-(\xi-m)/\eta]^4 \tag{13}$$

It satisfies the boundary condition [Eq. (4)] in the premelt heating regime, and Eq. (9) in the melting and melt-removal regime.

Since the temperature distribution [Eq. (11)] and the heat flowfield [Eq. (13)] are known, the following equation[6] derived from Biot's variational method is employed

$$\int_m^{\eta+m}\left\{(\theta-\theta_i)\frac{\partial\theta}{\partial\eta}+\dot{H}\frac{\partial H^*}{\partial\dot{\eta}}\right\}\mathrm{d}\xi=\left\{(\theta-\theta_i)\frac{\partial H^*}{\partial\eta}\right\}_{\xi=m} \tag{14}$$

Using Eqs. (11) and (13), Eq. (14) in the unknown generalized coordinate η becomes

$$\eta[(4/112)\dot{\eta}(\theta_1-\theta_i)+(11/12)\dot{m}(\theta_1-\theta_i)+(3/144)\eta\dot{\theta}_1] =(5/14)(\theta_1-\theta_i) \tag{15}$$

A. Premelt Heating Regime ($\tau\le\tau_m, \eta\le\eta_m, \theta_1\le 1$)

In this regime, θ_1 is a function of time and its value is less than the melting temperature of the solid. As a result, there is no melting and the melt is not formed, giving $m=\dot{m}=0$. Equation (15) reduces to

$$4\eta[(9/8)\dot{\eta}(\theta_1-\theta_i)+(21/32)\eta\dot{\theta}_1]=45(\theta_1-\theta_i) \tag{16}$$

Since it contains two unknown generalized coordinates θ_1 and η, a second relation between these two coordinates is obtained using Eqs. (3) and (10).

$$\eta=3(\theta_1-\theta_i)/(\theta_a^4-\theta_1^4) \tag{17}$$

This equation gives the value for the maximum penetration depth ($\eta=\eta_m$) when $\theta_1=1$.

Substituting Eq. (17) into Eq. (16) yields an equation for the surface temperature

$$[(57/63)(\theta_1-\theta_i)(\theta_a^4-\theta_1^4)+(144/63)\theta_1^3(\theta_1-\theta_i)^2]\dot{\theta}_1 =(40/63)(\theta_a^4-\theta_1^4)^3 \tag{18}$$

The solution of Eq. (18) gives surface temperature time history in closed form

$$\begin{aligned}\tau=&(9/20)[(\theta_1^2-2\theta_1\theta_i+\theta_i^3)/(\theta_a^4-\theta_1^4)-\theta_i^2(\theta_i-1)/(\theta_a^4-\theta_i^4)]+C_1(1/\theta_1-1/\theta_i)+C_2\ell n\theta_i(\theta_a-\theta_1)/\theta_1(\theta_a-\theta_i)+C_3\{1/(\theta_a-\theta_1)\\&-1/(\theta_a-\theta_i)\}+C_4\{(\theta_a+\theta_1)/\theta_1-(\theta_a+\theta_i)/\theta_i\}+C_5\ell n\theta_i(\theta_a+\theta_1)/\theta_1(\theta_a+\theta_i)+C_6\{(\theta_1/(\theta_a+\theta_1)-\theta_i/(i_a+\theta_i)\}\\&-C_7\{(\theta_a-\theta_1)/\theta_1-(\theta_a+\theta_i)/\theta_i\}+C_8\{(\theta_a+\theta_1)^2/\theta_1^2-(\theta_a+\theta_1)^2/\theta_i^2\}-C_9\{(\theta_a-\theta_1)^2/\theta_1^2-(\theta_a-\theta_i)^2/\theta_i^2\}\\&-C_{10}\ell n\theta_1^2(\theta_a^2+\theta_i^2)/\theta_i^2(\theta_a^2+\theta_1^2)-C_{11}\{1/(\theta_a^2+\theta_1^2)-1/(\theta_a^2+\theta_i^2)\}+C_{12}\{\theta_1/(\theta_a^2+\theta_1^2)-\theta_i/(\theta_a^2+\theta_i^2)\}+C_{13}\{\tan\theta_1/\theta_a-\tan\theta_i/\theta_a\}\end{aligned} \tag{19}$$

where

$$C_1=(3B-A\theta_a)/4\theta_a^4,\quad C_2=-(2A\theta_a+2B+B\theta_a)/4\theta_a^5,\quad C_3=(B+A\theta_a)/4\theta_a^4,\quad C_4=(A\theta_a-3B)/4\theta_a^5,\quad C_5=(3B-2A\theta_a)4\theta_a^5,$$

$$C_6=(B-A\theta_a)4\theta_a^5,\quad C_7=2B/\theta_a^4,\quad C_8=C_9=B/8\theta_a^5,\quad C_{10}=A/2\theta_a^4,\quad C_{11}=A/2\theta_a^2,\quad C_{12}=B/2\theta_a^4,\quad C_{13}=3B/2\theta_a^5$$

with

$$A=21/160\theta_a^2 \qquad B=(36\theta_i^2-57\theta_i)/160\theta_a^2$$

This equation satisfies the initial condition [Eq. (2)]. To obtain the numerical solution of Eq. (18), it is integrated using Simpson's rule with the limit of integration varying from θ_i to 1. This limit is divided into 100 parts, each part being equal to $0.01(1-\theta_i)$. Such a procedure has been shown to yield accurate results.[3]

B. Melting and Melt-Removal Regime ($\tau>\tau_m, \eta>\eta_m, \theta_1=1$)

In this regime, $\theta_1=1$, $\dot{\theta}_1=0$, and m is a function of time. Using these, Eq. (15) becomes

$$(28\eta\dot{\eta}+77\,\dot{m}\eta)=280 \tag{20}$$

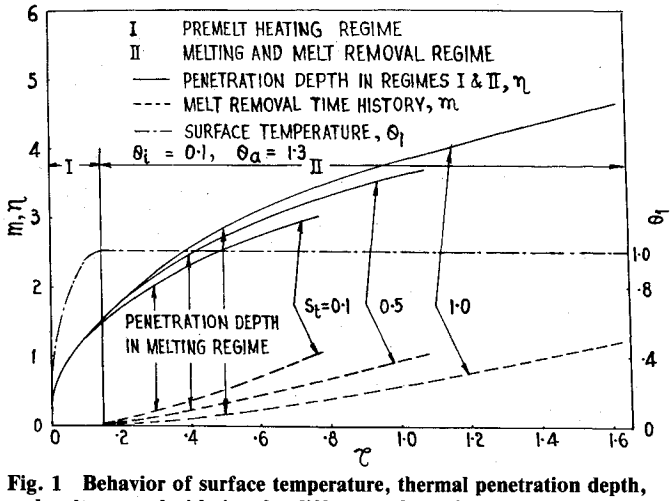

Fig. 1 Behavior of surface temperature, thermal penetration depth, and melt removal with time for different values of the parameter S_t.

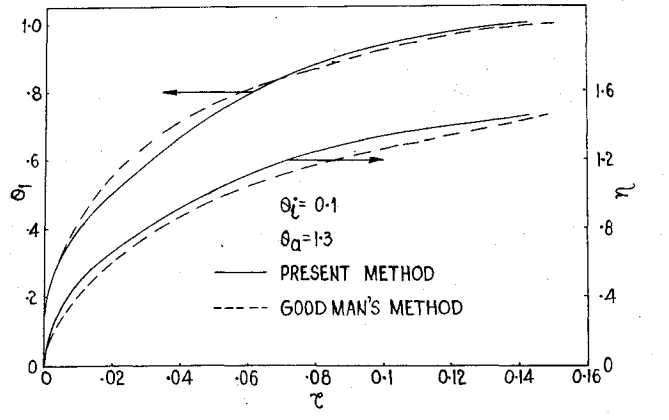

Fig. 2 Comparison between the present solutions and those of Ref. 4 in the premelt heating regime.

It contains two unknown generalized coordinates η and m. An auxiliary equation[3] relating these coordinates is obtained using Eqs. (10) and (13).

$$(\theta_a^4 - 1) = [(1-\theta_i) + S_t]\dot{m} + \tfrac{1}{4}(1-\theta_i)\dot{\eta} \tag{21}$$

Equation (20) together with Eq. (21) gives

$$\dot{\eta} = (A_1 - A_3\eta)/A_2\eta \tag{22}$$

$$\dot{m} = (A_5\eta - A_6)/A_4\eta \tag{23}$$

where

$$A_1 = 280[(1-\theta_i) + S_t],\quad A_2 = [35(1-\theta_i) + 112S_t]/4,$$

$$A_3 = 77(\theta_a^4 - 1),\quad A_4 = 4A_2,\quad A_5 = 112(\theta_a^4 - 1),$$

$$A_6 = 280(1-\theta_i)$$

Solving Eq. (22), its solution in closed form is given by the expression

$$\tau = \tau_m + (A_2/A_3)(\eta_m - \eta) + (A_1A_2/A_3^2)\ln(A_1 - A_3\eta_m)/(A_1 - A_3\eta) \tag{24}$$

It satisfies the initial condition [Eq. (6)]. Combining Eqs. (22) and (23) yields

$$\dot{m}/\dot{\eta} = dm/d\eta = A_2(A_5\eta - A_6)/(A_1 - A_3\eta)A_4 \tag{25}$$

Its solution gives a relation between m and η as

$$m = (A_2/A_3^2A_4)[A_3A_5(\eta_m - \eta) + (A_3A_6 - A_1A_5)\ln(A_1 - A_3\eta_m)/(A_1 - A_3\eta)] \tag{26}$$

When the time rate of depth of penetration becomes zero ($\dot{\eta} = 0$), Eq. (22) reduces to

$$\eta = \eta_s = A_1/A_3 \tag{27}$$

For the melting and melt-removal regime, it gives the maximum penetration depth because it satisfies the condition $d^2\eta/d\tau^2 < 0$. It is the solution of the steady-state penetration depth since $\dot{\eta}$ does not assume a negative value after this condition is attained. In this situation, the melt removal can be obtained using Eqs. (26) and (27).

Results and Discussion

Results obtained from the present analysis for time-dependent penetration depth, depth of melt removal, and surface temperature are shown graphically in Fig. 1 for both regimes. Regime I denotes the premelt heating regime and regime II represents the melting with the melt-removal regime. Regime I depends on initial temperature of the solid and the temperature of the surroundings, whereas regime II is controlled by a parameter S_t besides its dependence on these temperatures, which are taken to be 0.1 and 1.3, respectively, in the plot.

In regime I, Fig. 1 suggests that during the initial period of heating, the penetration depth increases very rapidly with a rapid increase in the surface temperature. This increase, however, shows with further elapse of time, and the surface temperature attains the melting temperature of the solid. Also, the premelt heating penetration depth η_m assumes a value of 1.456. This can be obtained using Eq. (17).

Figure 2 exhibits close agreement when these results are compared with the results of Goodman's approximate analysis based on a heat balance integral method.[4] However, the latter method overestimates by 4% the time for the surface to reach the melting temperature of the solid in comparison with the present method, even though a cubic temperature profile is taken in both methods. The relation between penetration depth and surface temperature given by Eq. (17) is the same as that obtained by Goodman's method.

The melting and melt-removal regime represented by regime II in Fig. 1 is a function of the inverse of the Stephan number. In the plot, the values of S_t are realistic for ablating materials.[5] It is observed that in the beginning of melting both η and m increase rapidly, for each value of S_t and m attain the steady-state value as η approaches the steady-state value. This result is found by employing Eq. (27). When S_t increases, η increases at any time τ, but the corresponding melt removal m decreases. This type of behavior was also observed by the present author for convective heating.[3]

Conclusions

The applicability of Biot's variational method has been extended to a problem of heating and melting with melt removal due to radiative heating. Solutions for both the premelt heating and the melting regime are found in closed form with the latter regime a function of the inverse of the Stephan number. In the premelt heating regime, the validity of the present results is demonstrated by comparing the present results with the results of a heat balance integral method.

References

[1] Biot, M.A. and Daughaday, H., "Variational Analysis of Ablation," *Journal of Aerospace Sciences*, Vol. 29, Feb. 1962, pp. 227-229.

[2] Biot, M.A. and Agrawal, H.C., "Variational Analysis of Ablation for Variable Properties," *Transactions of the ASME, Journal of Heat Transfer,* Ser. C, Vol. 86, 1964, pp. 437-442.

[3] Prasad, A., "Melting of Solid Bodies Due to Convective Heating with the Removal of Melt," *Journal of Spacecraft and Rockets,* Vol. 16, Nov.-Dec. 1979, pp. 445-448.

[4] Goodman, T.R., "Application of Integral Methods to Transient Nonlinear Heat Transfer," *Advances in Heat Transfer,* Vol. 1, 1964, pp. 55-122.

[5] Rohsenow, W.M. and Hartnett, J.P., *Handbook of Heat Transfer,* McGraw-Hill, New York, 1973, pp. 16-49.

[6] Yeh, L.T. and Chung, B.T.F., "Phase Change in a Radiating and Convecting Medium with Variable Thermal Properties," *Journal of Spacecraft and Rockets,* Vol. 14, March 1977, pp. 178-182.

A80-083

Axially Compressed Optimum Cylinder— Comparison of Stiffener Configurations

40013
40004

R. Karmakar*
Indian Institute of Technology, Kharagpur, India

VARIOUS authors have worked on the optimum design of waffle cylinders[1-8] with orthogonal and spiral stiffener configurations. This Note presents results of minimum weight design studies on six types of stiffener configurations for a given load intensity, cylinder length and radius (including a cylinder with bonded shell-wall construction). In the bonded construction thin sheets are folded so as to give a series of unidirectional stiffeners. Two such sheets are then bonded on either side of another thin sheet so that the stiffeners are placed orthogonally. Assuming perfect bonding such a cylinder can be treated as orthogonally stiffened.

The optimum equivalent thickness of a cylinder has been obtained through structural synthesis. The interior penalty function method[9] has been used with multiple starting points. The failure modes considered are: gross buckling,[10,11] buckling between circumferential stiffeners, local buckling of skin,[10,12] local buckling of axial and spiral stiffeners,[7,13] and yielding of the cylinder material. For a meaningful comparative study of the designs, the upper and lower limits of the design variables have been prescribed on a uniform basis (Table 1).

The fixed parameters for the designs have been taken as: cylinder length = 406.4 cm (160 in.), cylinder radius = 152.4 cm (60 in.), design load = 1755.55 N/cm (1000 lb/in.), $E = 7.326 \times 10^6$ N/cm^2 (10.6×10^6 psi), Poisson's ratio = 1/3, and yield stress = 49,763.6 N/cm^2 (72,000 psi). The results of the design studies are given in Table 2. For orthogonal stiffening the designs of Ref. 6 are lighter than those of the present study. The differences are due to the fact that in Ref. 6 the axial and circumferential stiffeners have unequal depths whereas in the present study the depths are equal. Stiffener depth is the most effective parameter in increasing gross buckling load. In automated design procedure, therefore, the stiffener depths tend to be large. With a large axial stiffener depth being restricted by stiffener buckling, circumferential stiffener depth tends to be large. This behavior can be observed in design study 6 (see Table 2) where d_c has moved very close to the prescribed upper limit. Since in the present study axial and circumferential stiffener depths are the same, skin thickness, the second most effective prarameter in increasing gross buckling load, tends to be large making the designs heavier. For spiral type outside stiffening the design of the present study is lighter than that of Ref. 6. The reason may be attributed to the higher estimation of skin buckling load in the present study.

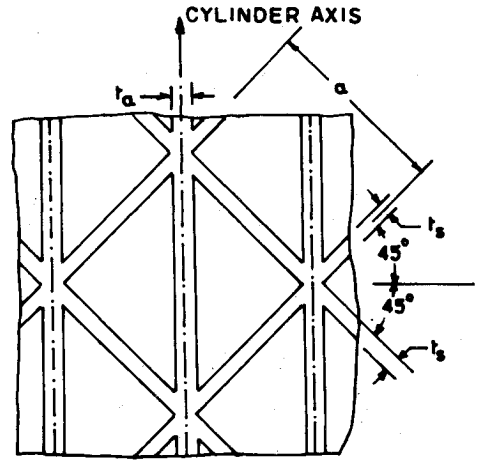

Fig. 1 Spiral-cum-axial type stiffening.

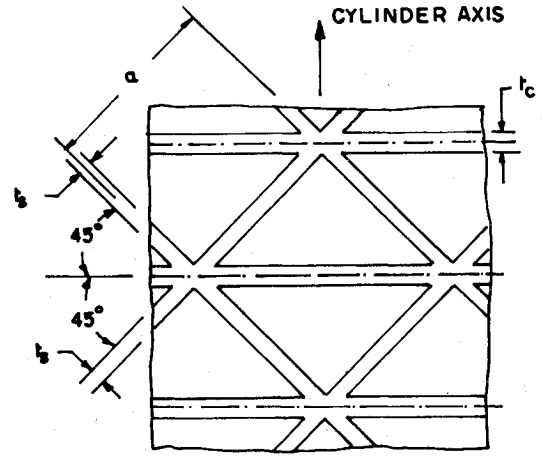

Fig. 2 Spiral-cum-circumferential type stiffening.

Outside stiffened waffle cylinders are found to be lighter than inside stiffened cylinders. Spiral-cum-axial (Fig. 1) and spiral-cum-circumferential (Fig. 2) stiffener configurations resulted in designs heavier than those with spiral stiffener configuration. For outside stiffener location, spiral type stiffening gives the lightest design followed by spiral-cum-circumferential type stiffening. For inside stiffener location, spiral-cum-orthogonal type (Fig. 3) stiffening gives the lightest design followed by spiral type stiffening. Among all the stiffener configurations considered for the waffle cylinder studied, spiral type outside stiffening gives the lightest design.

Folded sheet stiffening (Fig. 4) with axial stiffener on the inside (and circumferential stiffener on the outside) gives a design lighter than that with axial stiffener on the outside. It is also seen that folded sheet stiffening with axial stiffener on the inside gives a design which is only 0.85% heavier than that for spiral type outside stiffening.

Although the design studies have been limited to one cylinder and one load intensity, the studies demonstrate the significant effects of stiffener configurations and stiffener location on the minimum weight of a waffle cylinder. The result of the design study on folded sheet stiffening, the construction of which is likely to be cheaper than waffle construction, is encouraging.

Received Aug. 27, 1979; revision received March 28, 1980.

Index categories: Structural Design; LV/M Structural Design (including Loads).

*Lecturer, Department of Aeronautical Engineering.